The 6th International Supercritical CO_2 Power Cycles Symposium

March 27-29, 2018, Pittsburgh, Pennsylvania, USA

NUMERICAL SIMULATIONS OF SUPERCRITICAL CO_2 FLOW THROUGH PIPE BENDS: IDENTIFICATION OF A POTENTIAL CAUSE OF MATERIAL EROSION

Xiaoliang He
School of Mechanical, Industrial and Manufacturing Engineering
Oregon State University, Corvallis, Oregon 97331
Email: hexi@oregonstate.edu

Sourabh V. Apte
School of Mechanical, Industrial and Manufacturing Engineering
Oregon State University
Corvallis, Oregon 97331
Email: sva@oregonstate.edu

Ömer N. Doğan
National Energy Technology Laboratory
Albany, Oregon 97321
Email: Omer.Dogan@NETL.DOE.GOV

ABSTRACT

Supercritical Carbon Dioxide (sCO_2) has been proposed as working fluid for power generation cycles owing to its non-toxic, non-flammable properties, high density and low cost. The high-pressure (200-350 bar) and high-temperature (550-750°C) fluid enables extremely compact and high efficiency turbomachinery designs. However, there is evidence that even fairly pure sCO_2 flowing through turbomachinery at high mass flow rates can lead to material erosion. It was hypothesized that erosion may occur due to large fluctuations in wall shear stresses owing to turbulence and secondary flow patterns. To test this hypothesis, large-eddy simulation (LES) of a single-phase, turbulent flow of sCO_2 in a 90° pipe bend was performed at three different Reynolds numbers (5000, 27000 and 45000). The radius of curvature to pipe diameter ratio was chosen to be 1. First, the isothermal flow was validated against available experimental and numerical data. Shear stress on the pipe wall was computed and the power spectral density (PSD) was obtained. Besides, the snapshot proper orthogonal decomposition (POD) was applied to identify the secondary flow motions and the oscillation of the Dean vortices (i.e. swirl-switching). The swirl-switching was found to have the same oscillating frequency as that of the shear force. Consequently, it was reasonably conjectured that the swirling switching could be a cause of the erosion by generating the oscillation of the shear force on the pipe.

1 INTRODUCTION

Supercritical Carbon Dioxide (sCO_2) has been proposed as a working fluid for power generation in concentrated solar, fossil fuel and nuclear power plants. It is an ideal working fluid for power generation as it is non-toxic, non-flammable and low-cost fluid. The high-pressure (200-350 bar), high-temperature (550-750°C) and high-density fluid enables extremely compact and high efficiency turbomachinery designs. However, there are challenges unique to this technology. One of these challenges is erosion. Severe erosion has been observed in the sCO_2 power cycle test loops, particularly in the turbine nozzles and turbine blades [1]. It is conjectured that small metal particles and impurities in sCO_2 caused the erosion and failure of the blades.

It is also reported that even a fairly pure sCO_2 flowing through small pipe bends or junctions causes erosion of the material [2]. It is thus critical to identify potential sources of this erosion. For pure supercritical CO_2 flowing through pipe or duct bends, it is hypothesized that erosion may occur due to (i) large fluctuations in local temperature and pressure due to turbulence, secondary flow patterns, and property variations causing substantial shear stresses on the pipe walls, and (ii) surface or geometric irregularities impacting wall shear stresses and pressure variations.

To test these hypotheses and to gain better understanding of the stress distributions on the inner walls of pipe bends, predictive numerical simulation of a single-phase, turbulent flow with and without heat transfer in pipe bends at representative conditions and flow Reynolds numbers is performed in the present work. Considerable work exploring the dynamics of laminar and turbulent flow through pipe bends has been conducted [3–5]. Flow in curved pipes with bends involves flow turning that results in centrifugal forces on the fluid elements and corresponding pressure field to balance these forces. Formation of counter-rotating vortices, commonly termed as Dean vortices (Figure 1), are observed as the fluid elements with higher velocity are forced to the outside of the bend and lower velocity elements are forced toward the inside [3, 4]. These curvature-induced swirling motions and their strength is described in terms of the Dean number, De, where $De = \sqrt{D/2R_c}Re_D$. Here $Re_D = DU_b/\nu$ is the Reynolds number, D is the diameter of the pipe, R_c is the radius of curvature of the bend measured to the pipe centerline, U_b is the bulk velocity, and ν is the kinematic viscosity of the fluid. The unsteady behavior of Dean vortices (i.e. swirl-switching) and the time-scales related to oscillations of these vortices, reattachment point after the bend, and resultant variations in the shear stresses on the walls in turbulent flow have not been investigated thoroughly.

Rutten *et al.* [4] investigated turbulent flows in a 90° pipe bend using large-eddy simulations at Reynolds numbers of 5000–27000. Their work indicated that the overall forces on the pipe walls showed distinct peak in the power spectra related to the vortex shedding at the inner side of the bend. At large Re_D, the power spectra also exhibited frequency of oscillation much lower than the vortex shedding from flow separation. This was attributed to two Dean vortices whose strength vary in time dominating the flow field. This also suggests that local variation in the wall shear forces, especially after the bend, can be important in magnitude as well as time-scales. Such variations in local shear stresses may be relevant to the erosion problem, especially at very large Reynolds numbers.

Furthermore, Hellstrom *et al.* [5] used time-resolved stereoscopic PIV method to study turbulent flows at $Re_D = 20000$ and $Re_D = 115000$ through of a 90^o bend. Snapshot POD method was applied to identify the Dean motion and swirl-switching, as well as extracting the corresponding POD modes. The time coefficient of the first POD mode was found to be oscillating at the frequency, which is close to that of the overall force reported in Rutten *et al.* [4]. Although the Reynolds numbers of the two cases are not exactly the same, this leads to an open question that whether the swirl-switching can cause the oscillation of the shear forces on the pipe downstream of the bend, and indirectly be responsible for the material erosion observed.

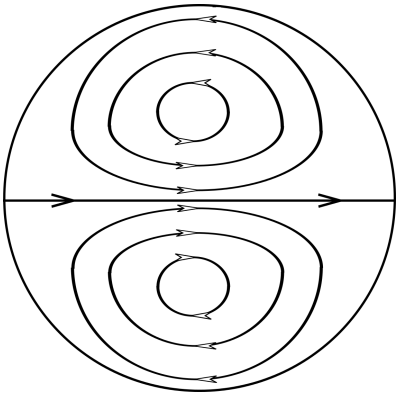

FIGURE 1: Dean vortices on the cross section plane of a pipe after the bend.

In the present work, we explore the turbulent flow through a 90° bend to first validate our results against those available from experiments as well as other simulations, and then investigate the nature of shear force variations at different locations after the pipe bend. In addition, the snapshot POD approach is implemented to detect the dominant POD modes and any frequency associated with the swirl-switching. The power spectral density functions are computed for both shear force and POD modes to reveal the connections between them. Future work will involve the thermal variation of properties of the fluid at high pressure and temperature, as well as at turbulent flows through different sections of the power plant, for example, turbine blades or nozzles.

2 NUMERICAL APPROACH

2.1 Mathematical formulation

In this section, the mathematical formulations for the single-phase LES with heat transfer are described. The mathematical formulation is based on the three-dimensional, variable density, low-Mach number equations for the fluid phase. Any acoustic interactions and compressibility effects are neglected. In addition, in writing the energy equation, we invoke the low-Mach number assumptions together. Also the viscous dissipation is assumed negligible. Radiative heat transfer is also neglected in this study. The Favre-averaged governing equations for LES of the zero-Mach number, variable density flow are given below,

$$\frac{\partial \overline{\rho_g}}{\partial t} + \frac{\partial \overline{\rho_g} \tilde{u_j}}{\partial x_j} = 0 \tag{1}$$

$$\frac{\partial \overline{\rho_g} \tilde{u_i}}{\partial t} + \frac{\partial \overline{\rho_g} \tilde{u_i} \tilde{u_j}}{\partial x_j} = -\frac{\partial \overline{p}}{\partial x_i} + \frac{\partial}{\partial x_j}\left(2\overline{\mu}\tilde{S_{ij}}\right) - \frac{\partial q^r_{ij}}{\partial x_j} \tag{2}$$

$$\frac{\partial \overline{\rho_g} \tilde{h}}{\partial t} + \frac{\partial \overline{\rho_g} \tilde{h} \tilde{u_j}}{\partial x_j} = \frac{\partial}{\partial x_j}\left(\overline{\rho_g}\tilde{\alpha}_h \frac{\partial \tilde{h}}{\partial x_j}\right) - \frac{\partial q^r_{hj}}{\partial x_j} \tag{3}$$

where

$$\tilde{S_{ij}} = \frac{1}{2}\left(\frac{\partial \tilde{u_i}}{\partial u_j} + \frac{\partial \tilde{u_j}}{\partial u_i}\right) - \frac{1}{3}\delta_{ij}\frac{\partial \tilde{u_k}}{\partial x_k}, \tag{4}$$

and $\tilde{\rho_g}$ is the density of the fluid, $\tilde{u_i}$ is the velocity, $\overline{\mu}$ is the viscosity, $\overline{p}$ is the pressure, $\tilde{\alpha_h}$ is the thermal diffusivity and the total enthalpy $\tilde{h}$ is given as

$$\tilde{h} = \tilde{h}_{\text{ref}} + \int_{T_{\text{ref}}}^{T} C_p(T)dT \tag{5}$$

. In the limit of zero-Mach number assumption, the thermodynamic pressure field within the domain remains constant at some reference value (250 bar used for sCO_2 calculations). The density of the fluid is then simply a function of the temperature, and an ideal gas-law is used in the present work. The fluid properties for supercritical CO_2 vary with temperature and are considered in the calculations. The property variations of real sCO_2 at 250 bar and the polynomial fits are given in Figures 2(a-d). The temperature typically of interest in sCO_2 heat exchangers ranges from 900-1000 K, far away from the critical point. It can be observed that the sCO_2 properties do not change significantly in such temperature range. Thus, the ideal gas law is appropriate for the present study.

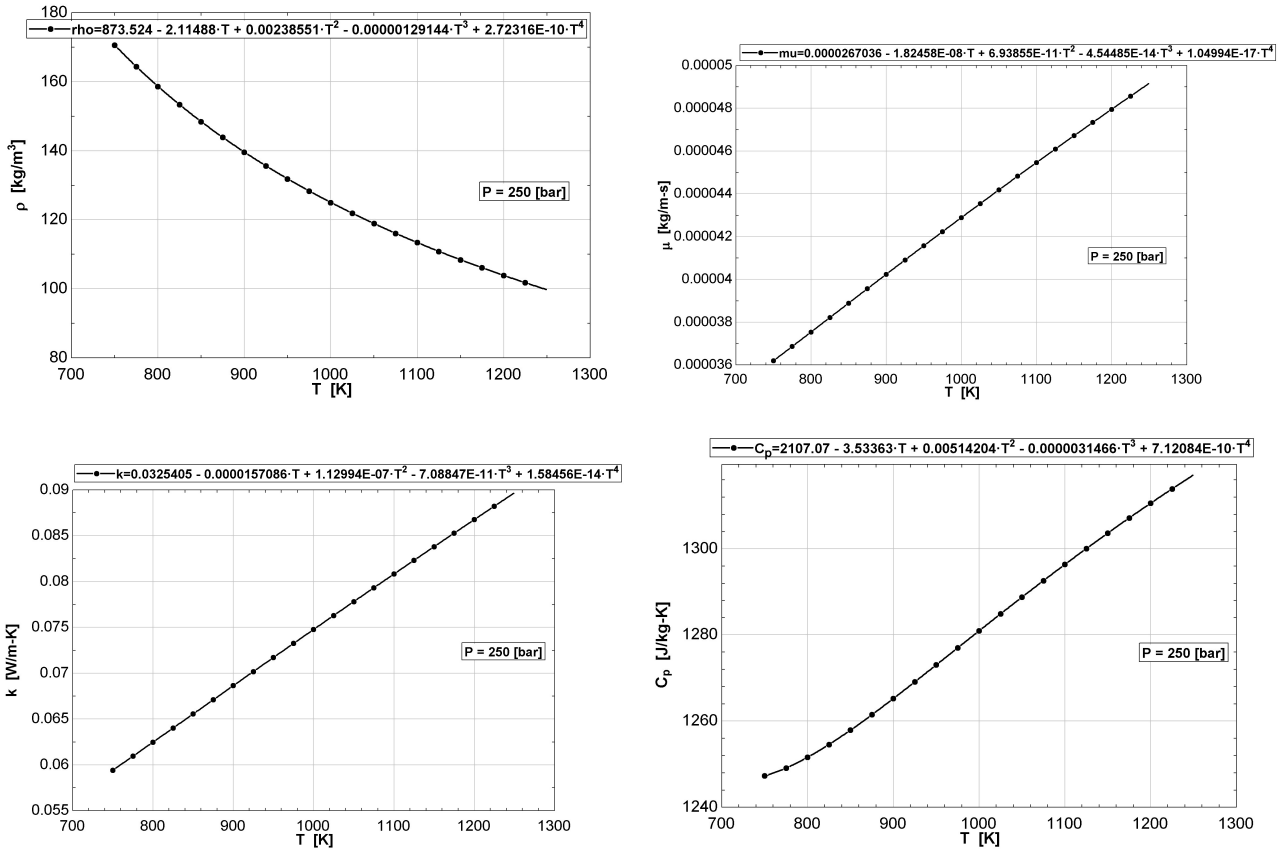

FIGURE 2: Variation of properties of sCO_2 at 250 bar over the temperature range of 700-1300 K.

The subgrid scale unclosed transport terms in the momentum, scalar, and enthalpy equations are grouped into the residual stress q^r_{ij}, and residual flux of enthalpy q^r_{hj}. The dynamic Smagorinsky model by Moin et al. [6,7] is used. The dynamic model has no adjustable constants, and thus allows evaluation

of the predictive capability of the model. The subgrid scale stress, q^r_{ij} is modeled as,

$$q^r_{ij} = \overline{\rho}(\tilde{u}_i\tilde{u}_j - \widetilde{u_i u_j}) = 2\mu_t \tilde{S}_{ij} - \frac{1}{3}\overline{\rho} q^2 \delta_{ij}, \tag{6}$$

where the isotropic part of the subgrid stress q^2 is absorbed into the pressure term, and the subgrid viscosity μ_t is given as

$$\mu_t = C_\mu \overline{\rho}\overline{\Delta}^2 \sqrt{\widetilde{S_{ij}}\widetilde{S_{ij}}}. \tag{7}$$

Here, $\overline{\Delta}$ is the filter width and the coefficient C_μ is obtained using least-squares approach following the dynamic procedure [8]. Similarly, the subgrid scale term in the enthalpy equation is modeled as,

$$q^r_{hj} = \overline{\rho}(\tilde{h}\tilde{u}_j - \widetilde{hu_j}) = \overline{\rho}\alpha_t \frac{\partial \tilde{h}}{\partial x_j} \tag{8}$$

$$\text{where} \quad \overline{\rho}\alpha_t = C_\alpha \overline{\rho}\overline{\Delta}^2 \sqrt{\widetilde{S_{ij}}\widetilde{S_{ij}}} \tag{9}$$

and the coefficient C_α is also obtained using the dynamic procedure.

2.2 Numerical solver scheme

An energy-conserving, finite-volume scheme for unstructured, arbitrarily shaped grid elements is used to solve the fluid-flow equations using a fractional step algorithm [6, 7, 9]. The velocity and pressure are stored at the centroids of the volumes. The cell-centered velocities are advanced in a predictor step such that the kinetic energy is conserved. The predicted velocities are interpolated to the faces and then projected. Projection yields the pressure potential at the cell-centers, and its gradient is used to correct the cell and face-normal velocities. A novel discretization scheme for the pressure gradient was developed by Mahesh *et al.* [6] to provide robustness *without numerical dissipation* on grids with rapidly varying elements. This algorithm was found to be imperative to perform LES at high Reynolds number in complex flows. The overall algorithm is second-order accurate in space and time for uniform orthogonal grids. A numerical solver based on this approach was developed and shown to give very good results for both simple [10] and complex geometries [7] and is used in the present study [11]. A thorough verification and validation of the algorithm was conducted [12, 13] to assess the accuracy of the numerical scheme for test cases involving two-dimensional decaying Taylor vortices, flow through a turbulent channel and duct flows [12] and particle-laden turbulent flows [7, 10].

3 COMPUTATIONAL SETUP

3.1 Pipe bend geometry

The computational setup used consists of a circular cross-section pipe with a 90° bend as shown in Figure 3. The pipe consists of a straight section of length $8D$, followed by the bend section and another straight section of $8D$ length. The bend with the curvature ratio of $R_c/D = 1$ is investigated. Owing to the bend geometry an unstructured grid with predominantly hexagonal mesh is used for calculations. When conducting large-eddy simulations, to create proper turbulence structure and velocity

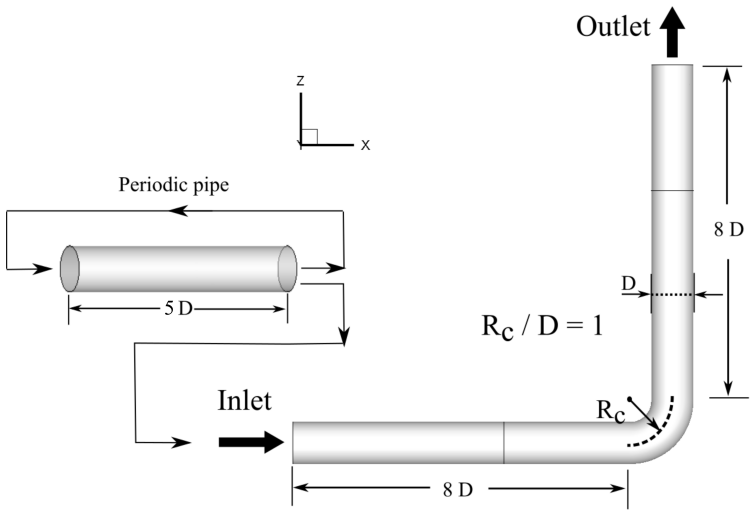

FIGURE 3: Schematic diagram of the computational setup for the 90° pipe bend with curvature ratio $R_c/D = 1$.

fluctuations, it is important to impose consistent fluctuations in the velocity field at the inlet [14]. Use of random fluctuations scaled with turbulence intensity values; however, can lead to convergence issues in a conservative numerical solver. A separate periodic pipe flow (length $5D$, see Figure 3) is simulated at the desired mass-flow rate and Reynolds number using a body-force technique [14]. The velocity field obtained from this periodic pipe flow simulation is stored at a single plane every time-step and is used as the inlet condition for the pipe bend. This provides a fully developed, instantaneous, turbulent velocity profile at the inlet of the pipe bend. A convective outlet condition is enforced at the outlet. In this study, only an isothermal flow field is simulated and thus effects of temperature and density variations and properties of sCO_2 are not included. Later study involves turbulent flow with heat transfer where these effects do become important.

TABLE 1: Grid resolutions in wall units for three different Reynolds numbers

	Δr^+_{min}	$(\Delta r\phi)^+_{max}$	$\Delta z^+_{min/max}$
$Re_D = 5300$	0.8	6.0	20/25
$Re_D = 27000$	1.13	21.4	20/25
$Re_D = 45000$	1.77	31.5	30/38

3.2 Grid resolution

The flow fields simulated are for three different Reynolds numbers, $Re_D = 5300$, $Re_D = 27,000$ similar to the work by Rutten *et.* [4] and $Re_D = 45000$. The grid resolutions for three different Reynolds numbers are listed in Table 1. Stretched grids are used in the wall normal (radial) direction with a minimum grid resolution near the wall in wall units of $\Delta r^+ \sim 0.8$ for $Re_D = 5300$, less than 2 for $Re_D = 27000$ and 45000. Nearly uniform grids are used in the axial direction with a resolution of $\Delta z^+ \sim 20$ for both $Re_D = 5300$ and 27000, while above 30 for $Re_D = 45000$. The maximum resolution

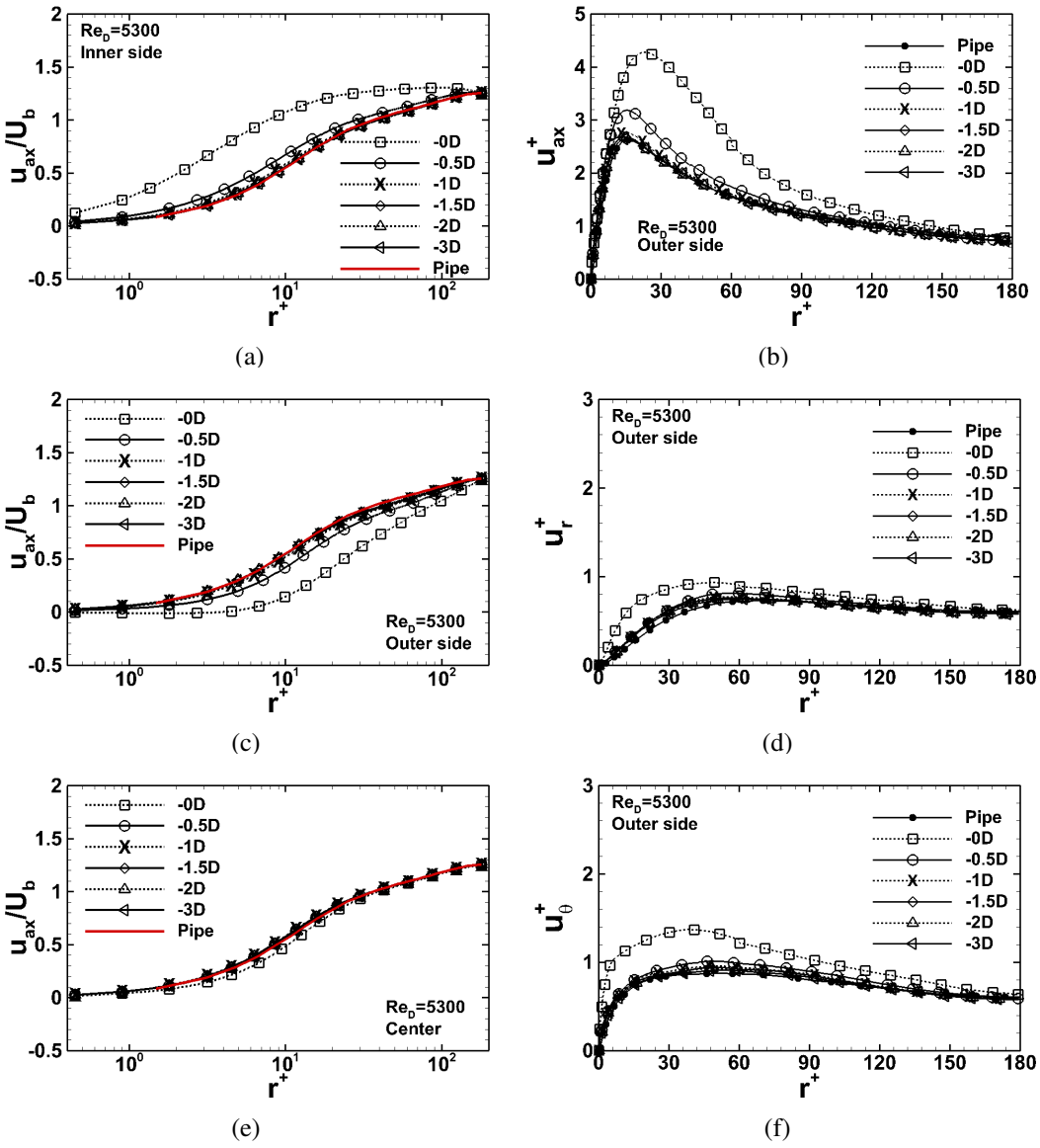

FIGURE 4: $Re_D = 5300$ mean velocity profiles normalized by bulk velocity along the (a) inner side, (c) outer side and (e) central in between of the pipe; and RMS velocity profiles in wall units along the outer side for velocity components in (b) axial, (d) radial and (f) circumferential directions.

in the circumferential direction is on the order of $(r\Delta\theta)^+ \sim 6$ for $Re_D = 5300$, around 20 for $Re_D = 27000$ and 31 for $Re_D = 45000$. These resolutions are finer than those used by Rutten *et.* [4]. In the present wall-resolved large-eddy simulation, no-slip conditions are applied at walls.

4 Results and Discussions

4.1 Validation results

In order to validate the flow solver for this flow configuration, first the mean velocity and RMS velocity profiles of $Re_D = 5300$ at different locations before the bend are plotted in Figure 4. "Inner side" means the profile is plotted along the inner side line of the pipe, and likewise the "outer side" and "center". It is observed that the mean velocity profiles before 1D of the bend all collapse together, and

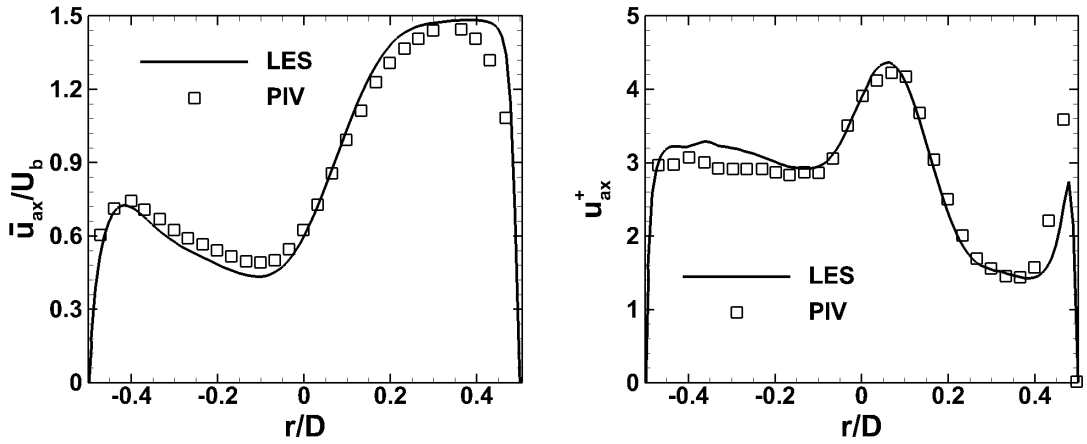

(a) (b)

FIGURE 5: (a) Mean velocity profile normalized by bulk velocity along the central line at 1D downstream the bend of $Re_D = 5300$; and (b) RMS velocity profile.

coincide with that of a fully developed straight pipe. This is consistent with what has been observed that the flow is not influenced by the bend before one diameter of the pipe [15]. The same characteristic can be obtained from RMS velocity profiles as well. The velocity profiles in Figure 4 are compared with [4], where the same Reynolds number flow was simulated. And they are in a good agreement.

Then, the velocity profiles at downstream of the bend are shown in Figure 5. The LES data are compared with PIV data from [16]. The mean velocity distribution is very well predicted by the simulation with a maximum 7% off. And the RMS velocity provides a reasonable good description comparing with the PIV data, with some expected deviation near the wall. This is due to the filtering process of LES modeling where some small flow structures were smeared out at the near wall region.

4.2 Flow field

Figure 6 (a) and (b) show the contours of the instantaneous and mean velocity magnitude fields normalized by the bulk velocity receptively. The general trend of the flow field can observed. The high velocity region from the straight pipe first gets closer to the inner wall starting about 1D before the bend. Then after about 30^o of curvature angle, it deviates from the inner wall, moves towards the outer wall and keeps this way downstream. This flow feature is consistent with what was reported in [17].

4.3 The POD analyses

Proper orthogonal decomposition (POD) is capable of extracting optimal modes from any field being examined. In other words, the optimal basis vectors are computed that can best represent the given data. The snapshot POD method can greatly reduce the computational comparing with the original POD approach. Hence, this method has been widely used in the fluid dynamics to detect the coherent structures and flow patterns ([5,18]). In this work, the mathematical formulations of the snapshot POD method described in [19] are adopted and briefly discussed in the following. For any given vector field $\mathbf{q}(\mathbf{x},t)$ with the temporal mean $\overline{\mathbf{q}}(\mathbf{x})$ removed, the remaining fluctuation part can be decomposed as:

$$\mathbf{q}(\mathbf{x},t) - \overline{\mathbf{q}}(\mathbf{x}) = \sum_j a_j(t)\,\phi_j(\mathbf{x}) \tag{10}$$

where, ϕ_j represents the POD modes, and a_j the corresponding time coefficients.

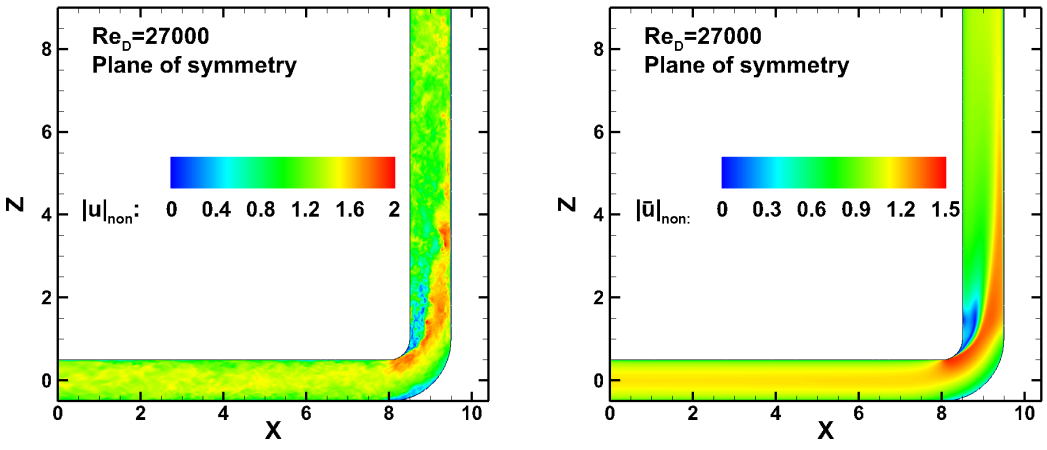

(a) (b)

FIGURE 6: Contours of (a) the instantaneous velocity magnitude field; (b) the temporal mean velocity magnitude field for $Re_D = 27000$

The POD mode is defined as a function of location only; while the temporal coefficient depends on time. In this way, the unsteady components of the vector field $\mathbf{q}(\mathbf{x},t)$ is decomposed into temporal and spatial domains respectively.

In this work, the velocity fields at three different locations: 1D, 3D and 5D after the bend are investigated using the snapshot POD method. The snapshots of the velocity fields at these locations are recorded in the specific frequency that is much higher than the target frequency of the POD modes to avoid aliasing. The first three modes are the most energetic ones and are illustrated in Figure 7. The first mode is a single cell covering the whole domain, representing the swirl-switching. Because the POD analysis is orthogonal, the direction of the mode could be reversed. And the Dean-like motion is recovered in the second and third modes, indicting that the Dean vortices have less energy and are weaker than the swirl-switching. In fact, the Dean-like motions could be seen as the transient period of the swirl-switching. These features are present regardless of the locations and Reynolds numbers. Also, the modes found are very similar to what were shown in [5, 18].

Moreover, the power spectral density (PSD) functions for the time coefficients a_j obtained at 1D after the bend for $Re_D = 27000\,\&\,45000$, representing the temporal characteristics of the POD modes, are computed and plotted in Figure 8 (a) and (b) respectively. In order to reduce the noise and focus on the targeted frequencies, the Bartlett window is used to filter the signals with degree of freedom of 60. The X axis is the Strouhal number (St), calculated by normalizing the frequency ($St = fD/U_b$). A very well pronounced peak at $St = 0.25$ is observed for $Re_D = 27000$, and it shifts to $St = 0.28$ at $Re_D = 45000$. Those distinguished peaks represent that the motion of swirl-switching is oscillating at such frequencies at the specific locations. Besides, the first and second modes are correlated by sharing the peak frequency, especially for the higher Reynolds number flow. This is another evidence that the Dean-like motions are associated with the swirl-switching.

4.4 Shear force

The shear forces caused by the fluid motions are obtained everywhere on the pipe surface. The overall forces are analyzed in the frequency domain to identify any oscillation. It is observed in Figure 8 (c) and (d) that the PSD has the peak frequency at $St = 0.25$ for $Re_D = 27000$ and $St = 0.28$ for

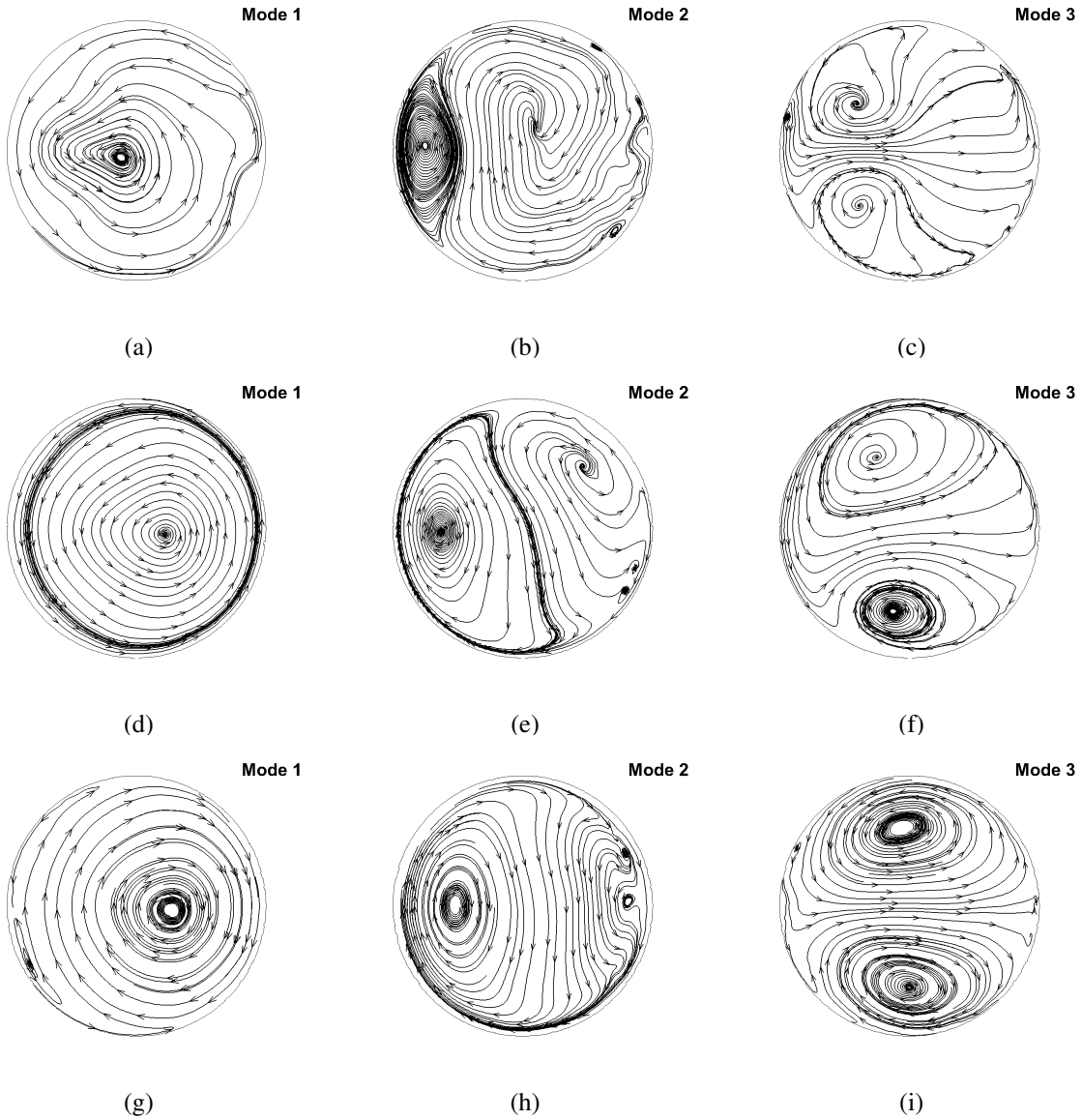

FIGURE 7: The first three POD modes at three locations for $Re_D = 27000$. The modes at the first line are at 1D downstream of the bend, second 3D and third 5D.

$Re_D = 45000$. These two frequencies are exactly matching with those of the POD modes. This is a strong evidence that the swirl-switching is highly correlated with the oscillation of the total shear force. This suggests that the turbulent flow induces oscillations of wall shear forces which can be a cause of the erosion, especially if the force magnitudes are large. For real sCO_2 power plant, the operating conditions can lead to extreme high Reynolds numbers ($\sim$ 20 million), and hence much higher shear forces. In addition, changes in temperatures and thermal properties of the fluid can influence the forces and their spectra as well.

5 Summary

Large eddy simulations of turbulent flow through 90° pipe bend with unit radius of curvatures ($R_c/D = 1$) were performed using an unstructured grid solver based on the principles of energy conservation. Flows at three different Reynolds numbers 5300, 27,000 and 45,000 were simulated to

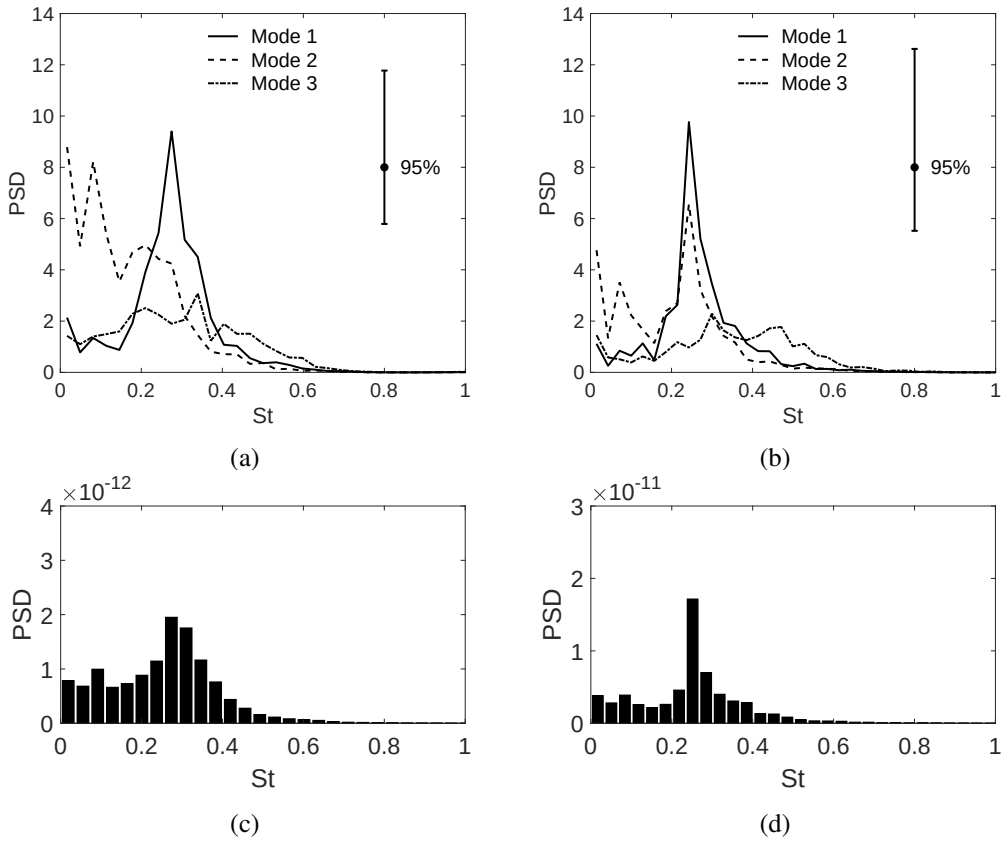

FIGURE 8: Power spectral density (PSD) functions for the time coefficients of the first three POD modes at 1D after the bend for (a) $Re_D = 27000$, and (b) $Re_D = 45000$; PSD of the overall shear force in X direction on the pipe for (c) $Re_D = 27000$, and (d) $Re_D = 45000$.

understand the behavior of the flow field within the pipe bends, the dynamics of the Dean vortices, variations in the shear stress. Specifically, the goal was to obtain the magnitude and time scale of shear stress and pressure variations on the pipe walls after the bend to identify their effects and potential role on erosion of the pipe material. It was hypothesized that erosion may occur due to large fluctuations in wall shear stresses owing to turbulence and secondary flow patterns. To test the hypothesis, first the solver was validated by comparing the mean and RMS velocity profiles before and after the bend with available experimental and numerical data. Then, the snapshot POD method was applied to detect the optimal modes, and identify the swirl-switching motion. The associated time coefficients were analyzed in the frequency domain to obtain its oscillating frequency. In addition, the shear forces on the pipe were computed and the power spectral density function was calculated as well. It was found that the swirl-switching has the same frequency as that of the oscillation of the shear stress. This was a strong evidence that the swirl-switching could possibly be the cause of the erosion by generating the oscillating shear forces on the pipe.

Acknowledgment

This work was performed in support of the US Department of Energy′s Fossil Energy Crosscutting Technology Research and Advanced Turbine Programs. The Research was executed through NETL Research and Innovation Center′s Advanced Alloy Development Field Work Proposal. This research was supported in part by an appointment (XH) to the NETL Research Participation Program spon-

sored by the US Department of Energy and administered by the Oak Ridge Institute for Science and Education. The use of the NETL's supercomputer Joule is also acknowledged.

Appendix-Surface roughness effect

The surface roughness does have an effect on the turbulent pipe flows, but it might be negligible for the present flow settings. The surface roughness (ε) of the pipe is estimated to be $10\mu m$. And the relative pipe roughness ($\frac{\varepsilon}{D}$) is then calculated to be $5E-5$. According to the Moody chart [20], for the present Reynolds number flows ($Re_D = 5000-45000$), the Darcy friction factors for the smooth pipe and pipe with relative roughness of $5E-5$ are almost the same. Thus, for the current study, the surface roughness does not have a significant influence. However, for the real applications, the Reynolds number could reach as high as 20 million. Then, the surface roughness plays a very important role for such type of flows. How to quantify the influence needs to be investigated in the future research.

REFERENCES

[1] Fleming, D., Kruizenga, A., Pasch, J., Conboy, T., and Carlson, M., 2014. "Corrosion and erosion behavior in supercritical co2 power cycles". In ASME Turbo Expo 2014: Turbine Technical Conference and Exposition, American Society of Mechanical Engineers, pp. V03BT36A002–V03BT36A002.

[2] Fleming, D., and Kruizenga, A., 2014. Identified corrosion and erosion mechanisms in sco2 brayton cycles. Report, Sandia National Laboratories.

[3] Berger, S., Talbot, L., and Yao, L., 1983. "Flow in curved pipes". *Annual Review of Fluid Mechanics,* ***15***(1), pp. 461–512.

[4] Rütten, F., Schröder, W., and Meinke, M., 2005. "Large-eddy simulation of low frequency oscillations of the dean vortices in turbulent pipe bend flows". *Physics of Fluids (1994-present),* ***17***(3), p. 035107.

[5] Hellström, L. H., Zlatinov, M. B., Cao, G., and Smits, A. J., 2013. "Turbulent pipe flow downstream of a bend". *Journal of Fluid Mechanics,* ***735***, p. R7.

[6] Mahesh, K., Constantinescu, G., Apte, S., Iaccarino, G., Ham, F., and Moin, P., 2006. "Large-Eddy Simulation of Reacting Turbulent Flows in Complex Geometries". *Journal of Applied Mechanics,* ***73***, p. 374.

[7] Moin, P., and Apte, S., 2006. "Large-Eddy Simulation of Realistic Gas Turbine-Combustors". *AIAA journal,* ***44***(4), pp. 698–708.

[8] Germano, M., Piomelli, U., Moin, P., and Cabot, W., 1991. "A dynamic subgrid-scale eddy viscosity model". *Physics of Fluids A: Fluid Dynamics,* ***3***, p. 1760.

[9] Mahesh, K., Constantinescu, G., and Moin, P., 2004. "A numerical method for large-eddy simulation in complex geometries". *Journal of Computational Physics,* ***197***(1), pp. 215–240.

[10] Apte, S., Mahesh, K., Moin, P., and Oefelein, J., 2003. "Large-eddy simulation of swirling particle-laden flows in a coaxial-jet combustor". *International Journal of Multiphase Flow,* ***29***(8), pp. 1311–1331.

[11] Apte, S., Dogan, O., and Ghodke, C. "Numerical investigation of potential erosion mechanisms in turbulent flow of sco2 pipe bends". In The 5th International Symposium- Supercritical CO2 Power Cycles.

[12] Shams, E., Finn, J., and Apte, S., 2011. "A numerical scheme for euler–lagrange simulation of bubbly flows in complex systems". *International Journal for Numerical Methods in Fluids,* ***67***(12), pp. 1865–1898.

[13] Shams, E., and Apte, S. V., 2010. "Prediction of small-scale cavitation in a high speed flow over an open cavity using large-eddy simulation". *Journal of Fluids Engineering,* ***132***(11), p. 111301.

[14] Pierce, C., and Moin, P., 1998. "Large eddy simulation of a confined coaxial jet with swirl and heat release". *AIAA Paper,* ***2892***.

[15] Vester, A. K., Orlu, R., and Alfredsson, P. H., 2016. "Turbulent flows in curved pipes: Recent advances in experiments and simulations". *Applied Mechanics Reviews,* ***68***(5), p. 25.

[16] Brücker, C., 1998. "A time-recording dpiv-study of the swirl switching effect in a 90 bend flow". In Proceedings of the Eight International Symposium on Flow Visualization, Sorrento, Italy.

[17] Sudo, K., Sumida, M., and Hibara, H., 2000. "Experimental investigation on turbulent flow through a circular-sectioned 180 degrees bend". *Experiments in Fluids,* ***28***(1), pp. 51–57.

[18] Vester, A. K., Orlu, R., and Alfredsson, P. H., 2015. "Pod analysis of the turbulent flow downstream a mild and sharp bend". *Experiments in Fluids,* ***56***(3), p. 15.

[19] Taira, K., Brunton, S. L., Dawson, S. T. M., Rowley, C. W., Colonius, T., McKeon, B. J., Schmidt, O. T., Gordeyev, S., Theofilis, V., and Ukeiley, L. S., 2017. "Modal analysis of fluid flows: An overview". *Aiaa Journal,* ***55***(12), pp. 4013–4041.

[20] White, F. M., 2011. *Fluid Mechanics (7th Edition).* McGraw Hill,2011.